PERGAMON

Deep-Sea Research I 49 (2002) 1741–1768

DEEP-SEA RESEARCH
PART I

www.elsevier.com/locate/dsr

Coupled 3D physical and biological modelling of the mesoscale variability observed in North-East Atlantic in spring 1997: biological processes

E.E. Popova[a,*], C.J. Lozano[b], M.A. Srokosz[a], M.J.R. Fasham[a], P.J. Haley[b], A.R. Robinson[b]

[a] *Southampton Oceanography Centre, Waterfront Campus, European Way, SO14 3ZH Southampton, UK*
[b] *Division of Applied Science, Department of Earth and Planetary Science, Harvard University, Cambridge, MA, USA*

Received 17 July 2001; received in revised form 15 February 2002; accepted 11 July 2002

Abstract

A limited area, eddy resolving coupled physical and biological model and data assimilation are used to reproduce and analyse the ecosystem variability observed in the North-East Atlantic in April–May 1997 on *Discovery* cruise 227. The ecosystem was in a post-bloom grazing controlled regime. The combination of the deep mixing in the upper layer during the cruise and a deeper than average winter convection led to high-nutrient–low-chlorophyll type conditions, which are unusual for this location. These conditions and lack of strong mesoscale physical features led to low spatial variability of phyto- and zooplankton yet strong sensitivity to the variations in the vertical mixing (storm event). Modelling results show that plankton patchiness formation under these conditions was dominated by biological mechanisms (mainly predator–prey oscillations). Furthermore, this mechanism, together with mixing and stirring, are responsible in this order for the observed scales and variability of patchiness from homogeneous low winter concentrations of phyto- and zooplankton.

Keywords: Modelling; Ecosystems; Mesoscale processes; Data assimilation

1. Introduction

Understanding the effect of physical processes on biological interactions in the upper ocean is a complex problem. Data gathered during interdisciplinary physical/biological mesoscale surveys are generally asynoptic, so that disentangling the effects of spatial and temporal variations is a non-trivial exercise. The best approach to the interpretation of such information is coupled biological and physical modelling and data assimilation. The purpose of such an approach is to provide a "motion picture" of dynamically consistent physical and biological 3D fields in close agreement with the observations. The model dynamics overcome deficiencies in the

*Corresponding author.
E-mail addresses: ekp@soc.soton.ac.uk (E.E. Popova), lozano@pacific.deas.harvard.edu (C.J. Lozano), mas@soc.soton.ac.uk (M.A. Srokosz), mjf@soc.soton.ac.uk (M.J.R. Fasham), haley@pacific.deas.harvard.edu (P.J. Haley), robinson@pacific.deas.harvard.edu (A.R. Robinson).

0967-0637/02/$ - see front matter
PII: S0967-0637(02)00091-2

Nomenclature

A	concentration of the ammonium (mmol m^{-3}), model state variable
α	initial slope of $P-I$ curve ($=0.04$ (W m^{-2})$^{-1}$ day^{-1}).
β_P, β_D	assimilation coefficients of zooplankton ($=0.75$, 0.75)
B_A	ammonium biological sources and sinks
B_P	phytoplankton biological sources and sinks
B_D	detritus biological sources and sinks
B_N	nitrate biological sources and sinks
B_Z	small zooplankton biological sources and sinks
D	concentration of the detritus (mmol N m^{-3}), model state variable
De_D	rate of breakdown of detritus to ammonium
De_P	rate of phytoplankton natural mortality
De_Z	rate of small zooplankton natural mortality
δ	fraction of the small zooplankton mortality transformed into ammonium ($=0.5$), the rest is instantly exported from the UML
E_Z	rate of small zooplankton excretion
G_P, G_D	grazing rates of the small zooplankton on the phytoplankton and detritus
G_{LP}, G_{LZ}	grazing rates of the large zooplankton on the phytoplankton and small zooplankton
g	small zooplankton maximum growth rate equal to 1.3 day^{-1}
I_0	photosynthetically active radiation (PAR) immediately below the surface of the water (assumed to be proportional to the absorbed total solar radiation at the sea surface with the coefficient 0.4)
J	light-limited phytoplankton growth rate
k_A	half-saturation constant for ammonium uptake ($=0.5$ mmol m^{-3})
K_N	half-saturation constant for nitrate uptake ($=0.5$ mmol m^{-3})
K_g	grazing parameter (0.8 mmol m^{-3})
K_w	light attenuation due to water ($=0.04$ m^{-1})
K_c	phytoplankton self-shading coefficient ($=0.03$ m^2 $mmol^{-1}$)
N	concentration of the nitrate (mmol m^{-3}), model state variable
μ_P	phytoplankton mortality rate ($=0.05$ day^{-1})
μ_Z	zooplankton mortality rate (0.2 day^{-1})
μ_D	detritus breakdown rate (0.05 day^{-1})
μ_e	zooplankton excretion rate (0.1 day^{-1})
Ψ	strength of ammonium inhibition of nitrate uptake (mmol m^{-3})$^{-1}$
P	phytoplankton biomass (mmol N m^{-3}), model state variable
p_P	relative grazing preference for phytoplankton ($=0.75$)
p_D	relative grazing preference for detritus ($=0.25$)
Q_N	non-dimensional nitrate limiting factor
Q_A	non-dimensional ammonium limiting factor
q	large zooplankton growth parameter (0.5 (day mmol m^{-3})$^{-1}$)
T	temperature (model state variable)
V_P	maximum growth rate of phytoplankton
w_g	detritus sinking velocity ($=4$ m day^{-1})
Z	small zooplankton biomass (mmol N m^{-3}), model state variable
Z_L	large zooplankton biomass (mmol N m^{-3}), model state variable
z	depth
z_i	depth of the model levels.

observations for some of the components of the ecosystem. Furthermore, the data driven simulations give an insight into aspects of the ecosystem processes, such as fluxes, that cannot be easily observed directly.

An even more challenging task for mesoscale biological modelling and data assimilation is to provide nowcasts and forecasts in real-time onboard for the optimisation of a cruise survey strategy (e.g. Robinson, 1992). The first example of a verified real-time primitive-equation (PE) shipboard physical forecast with data assimilation made for the Iceland-Faeroe front in August 1993 is described in Robinson et al. (1996), and a similar shipboard physical forecast coupled with a biological forecast made in June 2001 in the same area is described in Popova et al. (2002). To our knowledge, the first attempt to carry out a real-time biological forecast was made onboard RRS *Discovery* in the North-East Atlantic in April–May 1997 by L.A. Anderson and P.J. Haley (Srokosz, 1997). Here we present post-cruise simulations and analyses using a coupled physical–biological model with data assimilation for the data collected on the *Discovery* cruise 227 (hereafter abbreviated to D227).

Although physical data assimilation in 4D (space and time) models has been studied for over a quarter of a century, 4D biological data assimilation is still rarely attempted (Robinson and Lermusiaux, 2002). Some issues that require consideration were summarised by Anderson et al. (2000) in five groups: (i) spurious behaviour of model variables generated by non-smooth assimilation methods, (ii) excessive departures in biological variables from assimilated values due to inconsistency between model and data, (iii) need for interpolation and extrapolation of the available data (for example, downward extrapolation of satellite surface ocean colour data), (iv) artificial shock from apparent discrepancies between different data types, (v) necessity to assimilate all biological variables to avoid unrealistic values in non-assimilated variables.

The first two of the above are connected with the nature of biological models and the limitations of data assimilation methodologies. The three others result from scarcity of biological observations and difficulty of obtaining them with the same temporal and spatial resolution as that of the physical data. However, this list is not complete. Another issue is the fact that modelled biological variables (such as phyto- or zooplankton biomass) are not in fact directly measured quantities (e.g. fluorescence is used as a measure of chlorophyll-*a* (Chl-*a*) concentration, which in its turn is a measure of phytoplankton biomass).

Although it has been possible for some time to obtain high-resolution surveys of the phytoplankton field with an in situ fluorimeter fitted in towed undulators, similar measurements of zooplankton have only recently become possible with the advent of the Optical Plankton Counter (OPC). The D227 database represents one of the first examples of mesoscale surveying where high-resolution physical observations are available in parallel with measurements of major components of the ecosystem. High-resolution biological observations providing vertical structure of phyto- and zooplankton down to 300 m along the cruise track (with underway surface and deep CTD nitrate measurements) help to address the issue of scarcity and low quality of biological observations. This in turn highlights all the issues associated with (i) interpretation of modelling results in terms of measured quantities and (ii) high non-linearity of biological parameterisations. Thus, the D227 mesoscale experiment provides an opportunity for the testing of the diagnostic and predictive capabilities of different sorts of ecosystem models.

The advantages of a good biological data set do not make a modelling study of D227 a less challenging task. Biological conditions observed on D227 provided a challenging situation from the modelling point of view for the following reasons:

(i) The cruise location was chosen away from areas of energetic mesoscale variability such as fronts. Because of this, there were no clear correlations between spatial distribution of physical and biological characteristics, and thus the use of biological-temperature correlation (which sometimes provides a powerful tool for model initialisation and data

assimilation, e.g. Anderson et al. (2000), is not possible.

(ii) As will be shown later, the early stage of the spring phytoplankton bloom with its clear signal in all ecosystem characteristics was already over by the beginning of the cruise. Zooplankton biomass was high enough at the time to produce significant grazing pressure on phytoplankton. After a severe storm prior to the cruise and entrainment of nitrate, its concentration was very high (5–6 mmol $N\,m^{-3}$) and did not limit primary production. In such a grazing controlled (as opposed to nitrate limitation observed in the same area at the same time in 1989 (Fasham and Evans, 1995)) post-bloom condition, phytoplankton biomass varied little throughout the duration of the cruise suggesting a close balance between quite high primary production (our modelled values are about 0.5–0.7 mg $C\,m^{-2}\,day^{-1}$) and zooplankton grazing on phytoplankton. The phytoplankton dynamics at this period are driven by a balance between two nearly equal fluxes of opposite sign. The terms in the model representing these fluxes are highly non-linear and contain uncertain parameterisations and parameter values. In such a case, some inaccuracy in any of these terms may produce a fast growth or decline of phytoplankton which is very far from the observed behaviour.

The ecosystem behaviour observed during D227 which we define as "grazing controlled late-bloom" is an unusual case and is similar in its manifestations to the so-called high-nutrient–low-chlorophyll (HNLC) conditions typical of the Southern Ocean and North Pacific (caused there by the interplay of light, grazing and iron limitations, e.g. Baar and Boyd (2000)) but not reported before for 47°N in the North Atlantic. Previous measurements available for the spring time in this location show a strong spring phytoplankton bloom followed by nutrient depletion conditions (Bury et al., 2001; Lochte et al., 1993).

The purpose of this study is to try to reproduce the ecosystem variability observed during the D227 cruise in the framework of 4D modelling and data assimilation to answer the following questions: (i) To what extent we can describe observed mesoscale ecosystem variability using a simple biological model? (ii) What were the main mechanisms responsible for the formation of plankton patchiness observed during D227 cruise under the HNLC-type conditions and what was the reason for the occurrence of such conditions?

2. Discovery cruise No. 227

Discovery Cruise No. 227 was carried out to measure plankton patchiness in the eastern North Atlantic (in the area of 16–20°W, 47–49°N, Fig. 1a) during the period 15 April–16 May 1997. The primary objective of the cruise was to study the spatial variability of the biological activity in the upper layers of the ocean, and its relationship to the physical processes occurring there (Srokosz, 1997). One of the additional objectives was to demonstrate the feasibility of coupled biological and physical real-time shipboard nowcasting and forecasting. Hence the cruise plan was an attempt to find a compromise between an ideal survey structured for modelling and diagnostic studies.

Meteorological, physical, optical, chemical and biological measurements were made by using a combination of underway sampling, towed instrumentation and station sampling. A zig-zag search survey, two large-scale surveys and three small-scale surveys (Fig. 1b–f) were carried out during the cruise. The survey design included surveys at 30 km resolution of the entire area followed by surveys at 5 km resolution in smaller areas found to be biologically active (Srokosz, 1997). The large-scale surveys provide the data used here for initialisation, assimilation and verification.

Initialisation of the physical model required information about temperature and salinity profiles including deep layers below the reach of SeaSoar. Therefore, the first large-scale survey B (19.04.97–28.04.97) consisted of alternating lines of SeaSoar tows and 2000 m CTD stations. The survey legs had been spaced 30 km apart, with 180 km long survey lines and CTD stations every 30 km.

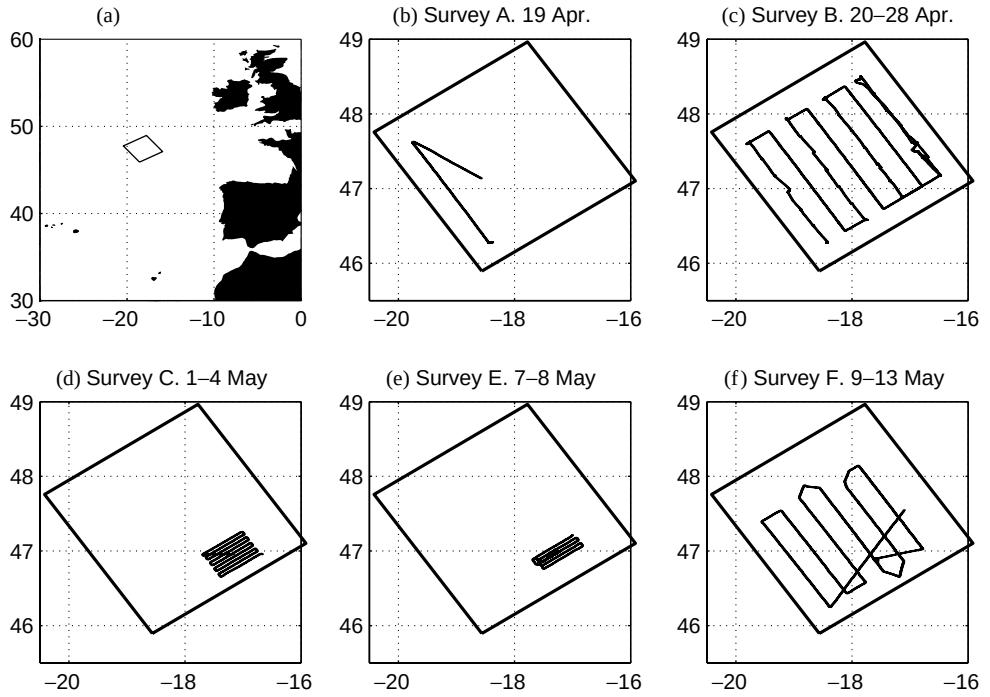

Fig. 1. Maps of the model area (thick line) and D277 cruise track (thin line): (a) North-East Atlantic location, (b) zig-zag search survey, (c) first (initialisation) large-scale survey B, (d) small-scale survey C, (e) small-scale survey E, (f) second (validation) large-scale survey F.

During Survey B an area of enhanced chlorophyll concentration was found towards the south-eastern boundary of the survey, and it was decided to carry out three repeated small-scale surveys in this region. For the small-scale SeaSoar surveys (C and E, Fig. 1) the survey legs had been spaced 5 km apart and were 60 km long. Bad weather conditions prevented the completion of one of the surveys (D). Survey C took under two days to complete, and survey E took slightly less than 1 day. The last large-scale survey F (intended to repeat the track of the first large-scale survey) was carried out with only SeaSoar. Because of time and weather constraints, this survey repeated only part of initial large-scale survey B, with lines of 150 km length. Thus two small-scale surveys resolve physical and biological variability on mesoscale (spatial scales characterised by the internal Rossby radius of deformation which was about 20 km in the cruise area), and two large-scale surveys provide a spatial context for evolution and propagation of the mesoscale features.

In this paper, we will discuss only those data used for initialisation and assimilation procedure, and comparison with the model run. The more detailed description of data collected during the cruise is given in Srokosz (1997), to which the reader is referred for further details.

Temperature and salinity measurements include 38 CTD stations (30 deep (down to 2000 m) taken mainly during survey B, 8 shallow (down to 300 m) taken in surveys C and E) and SeaSoar measurements down to 300 m.

Chl-*a* data used in this study were obtained with Chelsea fluorimeters attached to SeaSoar and CTD and from the pumped water supply. Because of the quenching effect (underestimation of fluorescence in the presence of light (Strass, 1990)) day time SeaSoar and CTD Chl-*a* profiles showed substantial subsurface maxima at the depth 20–40 m. Taking into account that none of

the nighttime profiles had subsurface maxima, and that the appearance of such maxima can be expected only under the conditions of nutrient limitation, we performed a simple correction of daytime profiles. For all profiles showing increase of Chl-*a* with depth, Chl-*a* distribution above subsurface maximum were considered to be homogeneous with value equal to this subsurface maximum. Although there are some more sophisticated approaches for quenching correction (Strass, 1990), a comparison of SeaSoar and underway measurements of Chl-*a* showed that for the purpose of this paper the simple correction applied here is adequate. It should be noted that as a result of our correction we obtained a lower estimate of the Chl-*a*, and daytime surface and subsurface values may be significantly underestimated mainly during the periods of the shallow diurnal upper mixed layer (UML) formation in which increased Chl-*a* concentration can be expected.

We used all available information about nitrate including 38 CTD profiles (15 depth levels each) and more than 500 underway samples gathered with the pumped water supply (5 m). Zooplankton data used in the simulations include mesozooplankton measured by OPC mounted on SeaSoar and microscopic measurements of microzooplankton from underway (5 m) bottle samples. OPC biovolume measurements were recalculated into biomass based on the assumption that zooplankton are approximately neutrally buoyant so $1\,cm^3$ of biomass is about 1 g wet weight. Of that 1 g wet weight, about 10% is dry weight and about 40% of the dry weight is carbon ($1\,cm^3\,m^{-3}$ of biovolume $\simeq 40\,mg\ C\,m^{-3}$, Parsons et al. (1977); Gallienne et al. (2001)). The OPC data were aggregated into four size classes: 250–500, 500–1000, 1000–2000, and $>2000\,\mu m$.

One hundred and twenty-eight samples of microplankton were collected during the cruise from the pumped water supply. Most cells were identified to species level, and others to genus level. Information about numerical dominance of species was used for the general analysis of the biological situation and stage of the bloom. Cell carbon estimates of the most common zooplankton species were used to derive microzooplankton biomass (O'Mahony, 1998).

Temperature, Chl-*a*, nitrate, micro- and mesozooplankton for 5 m depth measures during the cruise are shown in Fig. 2 in the form of temporal evolution. Objectively analysed values of temperature, chlorophyll-*a*, nitrate, micro- and mesozooplankton (size 250–500 and 500–1000 μm) for the depth 5 m for large-scale surveys are given in Figs. 3 and 4. Fields are mapped to the model grid along the cruise track. The objective analysis, which minimises the least-squares expected error, acts as an interpolator and as a smoother (Carter and Robinson, 1987; Lozano et al., 1996). The scales of the smoother are those of the decorrelation time and space scales used in the correlation function (A). The fields used for initialisation were obtained with a spatial decorrelation scale of 40 km and time de-correlation scale of 10 days. Space and time decorrelation scales for assimilation were set to 20 km and 5 days (initialisation and assimilation procedure will be explained in the next section).

3. The dynamical models

3.1. Harvard ocean prediction system

Reviews of the Harvard Ocean Prediction System (HOPS), a hierarchy of flexible and portable regional-to-basin scale ocean models, are given in Robinson (1996) and Lozano et al. (1996). HOPS consists of physical, biogeochemical and acoustic modules. Each have assimilation and initialisation schemes for their corresponding variables. The data analysis module of HOPS includes software components for the treatment of hydrographic data sets. Data are mapped onto regular grids via objective analysis (OA) schemes which interpolate via the minimisation of selected expected error norms (Robinson, 1996). The assimilation methodology used in HOPS is an intermittent optimal interpolation (OI) scheme developed by Dombrowsky and DeMey (1989). It consists of a series of linked cycles in which model and observation fields are combined together, taking into account the errors of prediction and observation, to form a better estimate of the field of interest (Robinson, 1996).

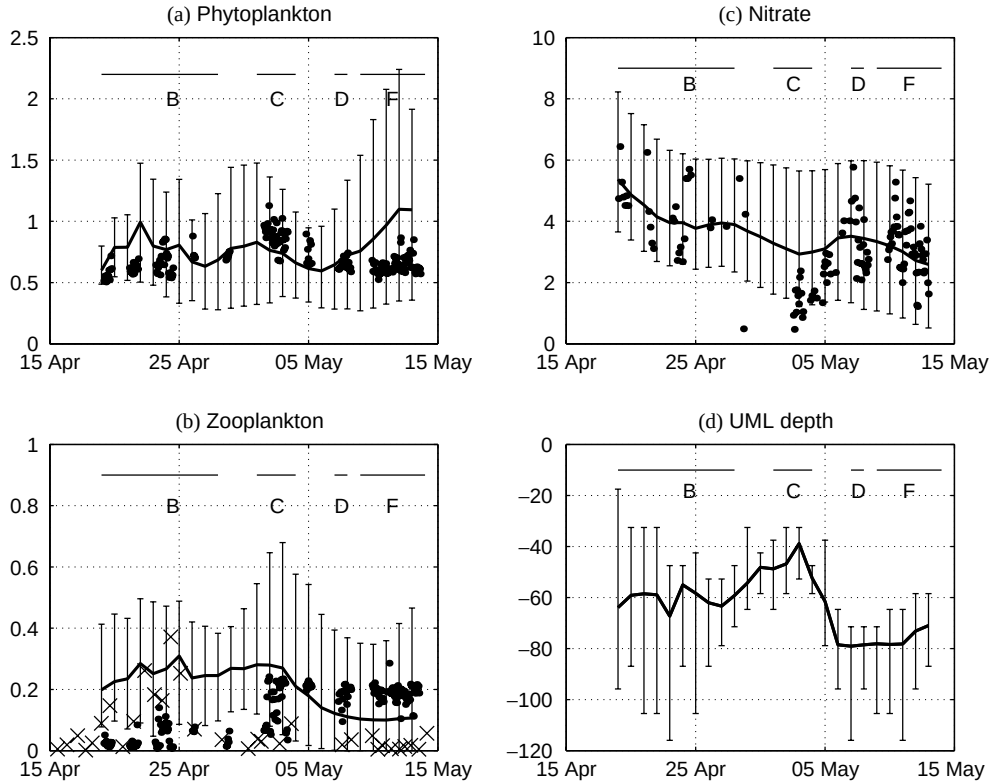

Fig. 2. Time evolution of the observed characteristics (dots) and modelled fields averaged over the model area (solid lines) for the 5 m depth. (a) Phytoplankton (mmol N m^{-3}), (b) Zooplankton (mmol N m^{-3}); dots are mesozooplankton (size (250–500 μm), crosses are microzooplankton (sum of these two types corresponds to the modelled zooplankton), (c) Nitrate (mmol m^{-3}), (d) UML depth (m) estimated as a depth at which temperature is 0.5°C less than the surface value. Vertical bars on the each graph show the range of variability over the model domain. Duration of the surveys (B, C, E, F) is shown above the each plot.

The HOPS primitive equation model is described in Spall and Robinson (1989), Robinson, (1996), Lozano et al. (1994, 1996). The dynamics are governed by the primitive equations under the hydrostatic, Boussinesq and rigid lid approximations. Subgridscale horizontal mixing of tracers, momentum, and vorticity are parameterised by applying a fourth-order (for tracers and momentum) and second-order (for vorticity) Shapiro (1970) filter once every time step. This filter is scale selective and removes two grid point waves, the small scales created by the enstrophy-cascade process of geostrophic turbulence (Rhines, 1979; Robinson and Walstad, 1987) and also any unresolved gravity waves. Vertical mixing of momentum and tracers are parameterised by the Richardson-number-dependent scheme of Pacanowski and Philander (1981). Convective mixing in the instances of local gravitational instability is handled by use of a local vertical diffusivity of 100 cm s^{-1}. The model uses the Orlanski (1976) radiation boundary conditions.

3.2. Biological model

The biological model used in this study is similar to Fasham et al. (1990) reduced to five variables: phytoplankton (P), zooplankton (Z), nitrate (N), ammonium (A) and detritus (D). Each is advected and diffused in the same manner as temperature (T) and salinity (S) and also modified by local exchanges between variables (biological sources and sinks) and sinking. The model equations are given in B.

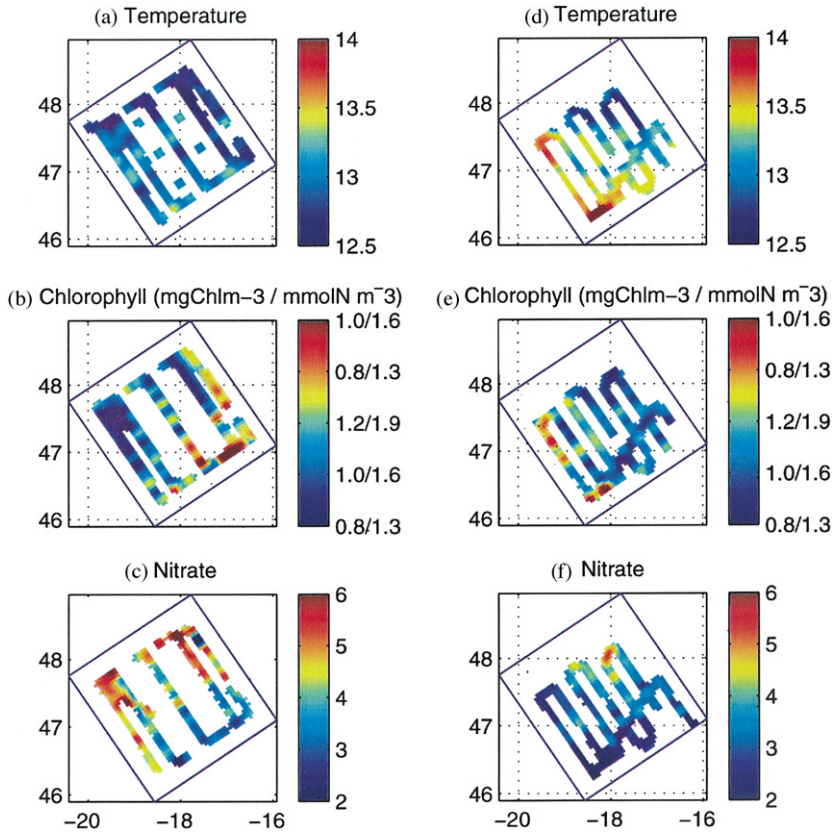

Fig. 3. Objectively analysed D227 data for the 5 m depth from surveys B (a–c) and F (d–f) mapped onto the model grid along the cruise track. (a, d) Temperature (°C); (b, e) Chl-*a* (given both in units of chlorophyll mg Chl m^{-3} and phytoplankton biomass mmol N m^{-3} with a chlorophyll to phytoplankton ratio of 1.6 mg Chl mmol N^{-1}); (c, f) Nitrate (mmol m^{-3}).

In our choice of the biological model we attempted to identify a minimum set of state variables to describe general features of the ecosystem during the D227 cruise. A $P-Z-N$ model, sometimes successfully used to describe general features of an ecosystem annual cycle, is too simple for a relatively short (about a month) time scale. Without an explicit description of detritus, instantaneous recycling of the organic matter in the UML would lead to overestimated regenerated production. A $P-Z-N-D$ model, in which N is dissolved inorganic nitrogen (nitrate and ammonium), may cause problems when nitrate concentrations become low and comparable to ammonium concentrations.

Here the zooplankton compartment is intended to encompass fast growing zooplankton, which include microzooplankton and the smallest class of mesozooplankton (less than about 500 μm). It has been shown in several studies that the phytoplankton dynamics are very sensitive to the parameterisation of the zooplankton loss term, which includes natural mortality and consumption by higher order predators (e.g. Fasham, 1993; Steele and Henderson, 1992). Since higher predators are not modelled explicitly, the effect of their grazing is prescribed by phyto- and zooplankton loss rates that do not depend on the population level of such predators. The linear form of these loss rates may be interpreted as representing a predator with a constant biomass, whereas a quadratic form may represent the effect of a predator whose biomass is proportional to that of modelled zooplankton and phytoplankton. Some

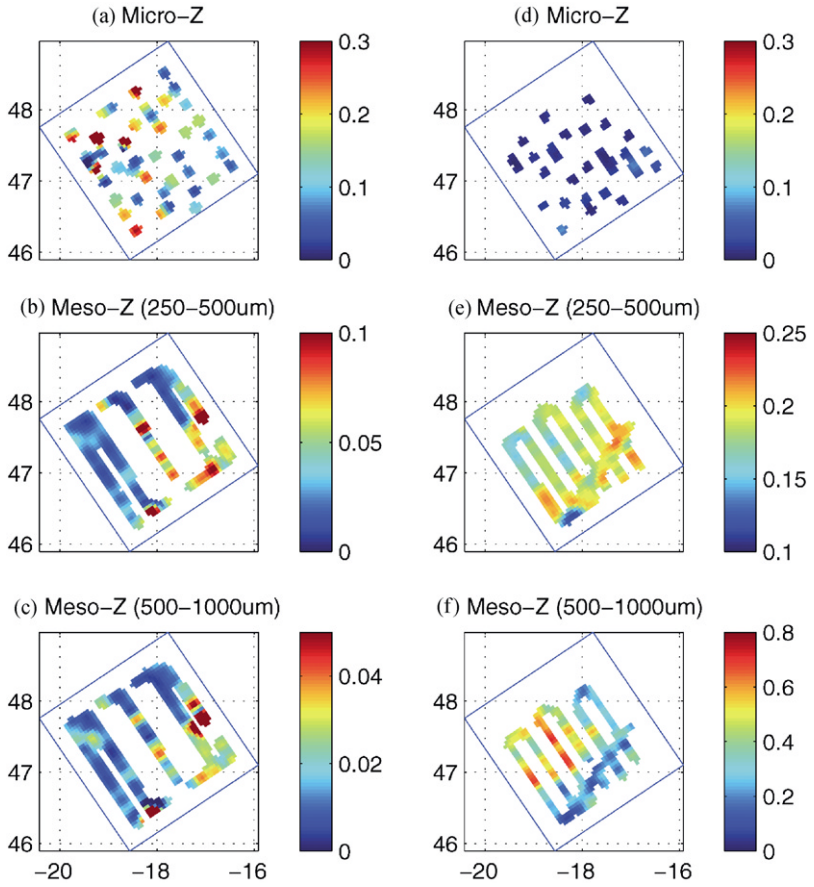

Fig. 4. Objectively analysed D227 data for the 5 m depth from surveys B (a–c) and F (d–f) mapped into the model grid along the cruise track. (a, d) microzooplankton biomass (mmol $N\,m^{-3}$); (b, e) zooplankton (size 250–500 μm) biomass (mmol $N\,m^{-3}$); (c, f) zooplankton (size 500–1000 μm) biomass (mmol $N\,m^{-3}$). Note differences in scales between surveys B and F.

other forms such as hyperbolic and sigmoid have been suggested (see Edwards and Yool (2000) for relevant discussion) to describe a more complex response. In this study, through experimentation, we also found extreme sensitivity to the parameterisation of the loss term. Furthermore, we were not able to describe the ecosystem dynamics correctly within the framework of a single (linear, quadratic, hyperbolic or sigmoid) form of this term. The approach taken here is described next.

From an analysis of OPC data it was found that during the first part of D227, the biomass of the 500–1000 μm size class of zooplankton was low (<0.05 mmol $N\,m^{-3}$) over the whole area and could not have had a profound impact on the rest of the ecosystem. During the second part of the cruise, over a significant part of the cruise area its biomass was more than 0.5 mmol $N\,m^{-3}$ (about two–three times higher than that of smaller zooplankton). Furthermore, its spatial distribution at some periods of time appeared to be in negative correlation with 250–500 μm size class (Fig. 4e and f). Such a feature could either be a manifestation of predator–prey oscillations, or advection of water masses with different ecosystem characteristics. In either case since larger zooplankton can exert a powerful control on smaller zooplankton dynamics and that in its turn on phytoplankton, any single parameterisation form described above

would probably fail to reproduce ecosystem behaviour in our case.

Here we have made an attempt to resolve this difficulty by dividing the zooplankton into two parts: the small zooplankton ($<500\,\mu m$ size) as a state variable Z; and the larger zooplankton imposed as an external tracer, Z_L, which is advected, diffused and provides a gazing pressure on Z and P but has zero biological sources and sinks. In our case Z_L was inferred from the measured (500–1000 μm size) zooplankton OPC data. The loss terms for small zooplankton and phytoplankton (see Eqs. (B.2) and (B.3) in Appendix B), include natural mortality, here represented with a linear term; the small zooplankton grazing of phytoplankton and the predation of large zooplankton on small zooplankton and phytoplankton. The predation terms are proportional to the modelled zooplankton (or phytoplankton) and the biomass of larger zooplankton (see Eq. (B.13) in the B). The large zooplankton are advected and diffused, but not altered by predation (Eq. (B.7)).

3.3. Model domain and external forcing

The model domain is centered at 47.4°N, 18.2°W, with a horizontal resolution of 5 km, a grid size $49\times51\times60$ and a rotation of -34° to align the grid with the cruise tracks. A vertical hybrid coordinate system (Lozano et al., 1994) is used with 53 flat levels overlying 7σ-levels providing resolution of 5 m in the upper 55 and 400 m near the bottom. A time step of 15 min is used.

The atmospheric fluxes included wind stresses derived from six hours' wind stress analyses from ECMWF, daily averaged water flux (evaporation minus precipitation), and one hours' surface heat flux and short-wave radiation derived from the US Navy NODDS product.

3.4. Overview of physical and biological situation

The first large-scale survey began on April 19. Two important factors should be mentioned about the physical and biological conditions that occurred before this date. The first is the large increase in the wind speed (up to $20\,ms^{-1}$) on April 17, which was presumably followed by a deepening of the UML and entrainment of nutrients. At this time of the year, when nutrients just below the UML are not yet depleted, mixing induced by a storm of such a strength brought their concentration almost back to the high winter level. The first survey began just at the beginning of the period of stabilisation of the UML, when its depth was still relatively deep (60–80 m).

The second important fact followed from microscopic analysis of plankton samples which suggested that the spring phytoplankton bloom had already occurred. *Chaetoceros spp.* from the Hyalochaete group can be used as a marker for the oceanic spring diatom peak, but very few of these species were present in any great numbers and no resting spores were recorded. The presence also of a diverse dinoflagellate population further supports the idea that the spring peak had already occurred. Flora was composed of post-spring peak species such as micoflagellates and small gymnodinium species, and species more indicative of a summer flora, such as species from the *Ceratium* genus, were also common (O'Mahony, 1998). Post-bloom conditions are also evidenced by colour data obtained by OCTS on ADEOS. In spite of significant cloud cover in March–April, weekly mosaics of ocean colour images give some overview of the spring bloom development in this part of the North-East Atlantic. Significant increase of Chl-*a* is obvious for the last week of March and first week of April. Starting from the second week of April Chl-*a* is low compared with the beginning of April and relatively constant.

By a coincidence, the four surveys of the cruise fell precisely into four different types of physical situations which determined different types of ecosystem behaviour. The first (large-scale) survey was carried out during a time of moderate (UML about 50–60 m) mixing. The second (small-scale) survey was under the conditions of low wind and very stable stratification with UML depth about 30–40 m. A strong storm occurred on May 5 (just after the completion of second survey) causing the UML to deepen to about 70–80 m, so that the impact of the storm was a dominant feature of the third (small-scale) survey. The fourth (large-scale) survey was carried out under the post-storm conditions with deep (70–80 m) UML, except for

the last day of the cruise (13 May) when stabilisation of the stratification began again with UML shallowing to 55–65 m.

We should also mention the first "search pattern" survey A (Fig. 1b), which was carried out using towed SeaSoar and took 1 day to complete. The first leg of this zig-zag survey had crossed the southwest part of the domain, and the second leg was identical with the first leg of survey B. Measurements from this survey were used to estimate the rate of change for nitrate, phyto- and zooplankton for use in the initialisation.

3.5. Initial biological and physical fields

Measured values of Chl-*a*, temperature, microzooplankton, nitrate and mesozooplankton of two size classes (250–500 and 500–1000 μm) for Survey B are given in Figs. 3a–c and Figs. 4a–c. Temperature distributions do not show the existence of strong mesoscale features nor associated with them large spatial gradients of biological properties. During Survey B, measured Chl-*a* values varied little over the survey area with values about 0.8–1 mg Chl m^{-3} with the exception of the southeast part of the domain, where concentrations of 1.2 mg Chl m^{-3} were found (Fig. 3b).

As a result of a storm prior to the cruise, the concentration of nitrate was relatively high throughout the area, with values between 3 and 5 mmol N m^{-3} (Fig. 3), so phytoplankton growth was not limited by nitrate availability. Small zooplankton (sum of microzooplankton shown in Fig. 4(a) and (d) and mesozooplankton (250–500 μm) shown in Fig. 4(b) and (e) did not show a link with the Chl-*a* field, although correlation between Chl-*a* and mesozooplankton (250–500 μm) is high.

The first large-scale survey B was designed to provide initial conditions for the model run. Taking into account that phytoplankton can easily double its concentration in 1 day under favourable conditions, the long (8 days) duration of this initial survey makes it a difficult task to distinguish between spatial and temporal variations along the cruise track. Initialisation fields created from a survey of such duration may lead to the appearance of artificially high spatial gradients. To account for the rate of change of the ecosystem characteristics due to the biological fluxes, we applied a temporal correction for biological fields as follows. Nitrate observations obtained from stations in close proximity during surveys A and B allow us to estimate changes in nitrate concentrations at nearly daily intervals for the period 19–24 April. In addition to this, part of the last (CTD) leg of survey B was repeated with SeaSoar and underway nitrate measurements. In this manner another estimate of nitrate rate of change was obtained for 27 and 28 April. The observations show that Chl-*a* concentration remained nearly constant in time, whereas nitrate had a stable rate of decrease of about 0.2–0.3 mmol N m^{-3} day^{-1}. Since there was no significant change in physical conditions (most importantly in the UML depth), we conclude that these features were typical during the entire period of survey B. A similar estimate of zooplankton rate of change shows no significant change of biomass although this estimate is less reliable. Due to the uncertainty of micorzooplankton measurements no correction was introduced to zooplankton biomass to avoid the emergence of an additional uncertain factor in the estimation. In conclusion we expect that during the first large-scale survey, the averaged primary production rate of about 0.2–0.3 mmol N m^{-3} day^{-1} was compensated by grazing, which in its turn was closely balanced by zooplankton excretion, natural mortality and grazing by larger zooplankton providing nearly constant zooplankton and phytoplankton biomass. Based on this assumption, we obtained initial estimates for the phytoplankton field from survey B Chl-*a* measurements with no correction necessary for a temporal trend. Data were objectively analysed and converted into phytoplankton biomass using a chlorophyll to phytoplankton ratio of 1.6 mg Chl mmol N^{-1} (based on about 50 gC (g Chl-*a*)$^{-1}$ ratio).

The model state variable Z is intended to represent fast-growing zooplankton with size < 500 μm. The initial estimate of this variable was obtained as a sum of objectively analysed fields of mesozooplankton of size range 250–500 μm as measured by OPC, and microzooplankton obtained through microscopic analysis. Since samples of microzooplankton were taken at

a single (5 m) depth and there was no additional information about their vertical distribution, we assumed that the typical vertical profile was of the same shape as that of Chl-*a*. In the same manner as for phytoplankton initial estimates, we used all data obtained for survey B and did not apply any correction for any temporal trend.

Initial estimates of the nitrate field were obtained from survey B underway nitrate measurements and CTD profiles extended from 2000 m down to the bottom using climatological information from Conkright et al. (1994). To put all the survey B measurements into correspondence with the initialisation time, we applied a depth-dependent nitrate change rate. The surface rate was 0.3 mmol N m^{-3} day^{-1} with a vertical profile of the same shape as non-dimensional profile of Chl-*a* multiplied by -1. This simple approach follows from a two-component ($N-P$) ecosystem mass balance and can be considered as a good approximation when no profile measurements of primary production are available.

The simple method of correction described above was based also on the assumption that the biological time scale during survey B (O(1 day)) was shorter than the advective scale (O(3 days)) and that vertical mixing remained relatively constant during survey B. If the cruise had been started, for example, 3 days earlier or later (in the first case capturing the deep storm-induced mixing, in the second case capturing rapid stabilisation of stratification), such a simple correction would not be sensible.

There were no D227 measurements for detritus and ammonium, and historical information for this area is scarce. We therefore assumed the initial ammonium concentration to be 5% of nitrate, and for initial detritus to be 20% of phytoplankton. Both estimates were taken from modelling results of Fasham and Evans (1995). Even though these estimates are somewhat arbitrary, we found that these ratios did not undergo significant changes during the model simulations and thus proved a posteriori to be reasonable estimates.

Initial fields of temperature and salinity were constructed from climatological information (the objectively analysed one degree mean monthly fields (April and May) from Levitus and Boyer (1994)) and the D227 T and S measurements obtained during the first large-scale survey. Geostrophic balance was assumed, and the geostrophic stream function was obtained by integration of the hydrostatic equation up and down from a chosen level of no motion (2000 m). Velocity fields were then computed from the thermal wind relationship.

4. The control run

The initialisation and assimilation methodology of our control experiment generally follows the approach employed by Robinson et al. (1996). The model run starts at 19 April, which corresponds to the end of the zig-zag survey and beginning of the initialisation survey. The model was initialised with data collected during survey B as described in the previous section. Since this survey lasted for 8 days, we can expect these initialisation fields to be substantially asynoptic. To overcome the asynopticity problem the same data interpolated with the smaller decorrelation scales were then assimilated on 20, 22, and 25 April when the ship was in the western, central and eastern parts of the domain correspondingly. Thus, the forecast domain was built up by a process of initialisation followed by three cycles of intermittent optimal interpolation in which model and observation fields are combined together, taking account the error field of objectively analysed data. At a time and place where an observation is present, the relative error value is zero, and far from the data the relative error value is one, time and space scales of error increase being determined by the de-correlation scales. The use of small decorrelation scales provides three-step insertion of the time-evolving measured fields into corresponding modelling time and space thus making the resulting field as synoptic as possible.

The model results for survey B we designate as a nowcast. The forecast was carried out from this buildup process.

4.1. Survey B (nowcast). "Regular" spring post-bloom conditions

Results of the nowcast for 27 April are given in Fig. 5. There is no clear link between temperature

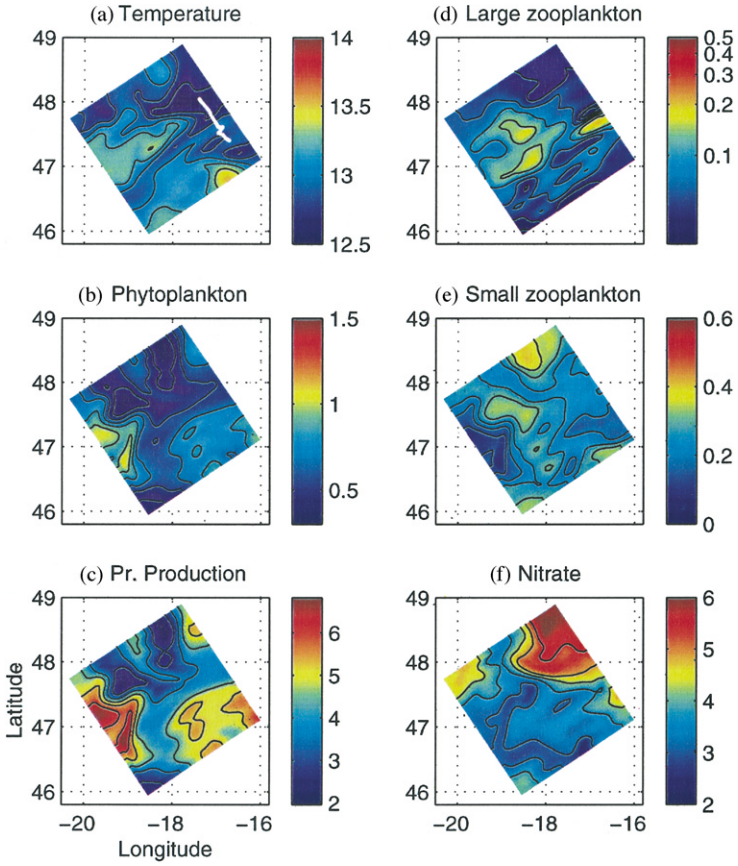

Fig. 5. Modelled horizontal fields (depth 5 m) of (a) temperature (°C), (b) phytoplankton (mmol N m^{-3}), (c) primary production integrated over 100 m (mmol N m^{-2} day^{-1}), (d) large zooplankton (mmol N m^{-3}), (e) small zooplankton (mmol N m^{-3}), (f) nitrate (mmol N m^{-3}), for 27 April (survey B). Ship position during this day is shown on the Temperature field (white line).

and ecosystem characteristics (except that relatively large-scale patterns of high nitrate concentration generally correspond to lower temperature values). This is not surprising. Strong physical–biological correlation can be expected for two reasons. The first is the presence of two water masses with different biological and physical characteristics (frontal area or advected mesoscale feature like an eddy). The second is when there are conditions of strong nutrient limitation, where in some places upwelling or entrainment of nutrients and temperature from below cause an increase in phytoplankton growth rate in parallel with a decrease in temperature. In our case, under the spring post-bloom conditions, the UML is still not nutrient depleted. Even if surface nutrients had been very low prior to the cruise, the storm event would have restored their concentration to a level well above limiting values. As seen from Fig. 5f, the nitrate concentration varies from 3.5 to 6 mmol m^{-3} and so phytoplankton growth rate is not nutrient limited. Temperature (Fig. 5a) and velocity (not shown) distributions do not indicate strong frontal or eddy-like structures; thus they do not provide a basis for a strong correlation between physical and biological spatial patterns, although the effects of stirring are evident in the biological fields.

Two areas of high phytoplankton biomass are located in the eastern and south-western parts of the domain (Fig. 5b) and correspond to lower zooplankton values (Fig. 5e), although clear

inverse correlation cannot be established for the whole area. This sort of correlation between P and Z again points to post-bloom conditions, when predator–prey oscillations are in the grazing-dominated stage. For the beginning of the spring bloom we should expect a clear positive correlation (zooplankton increase proportionally to the phytoplankton availability). As the bloom develops and zooplankton grazing pressure plays a major role (grazing-dominated stage, e.g. Ryabchenko et al. (1997), a mixture of positively and negatively correlated patches should be expected, depending on the temporal development of the zooplankton–phytoplankton coupling. To analyse this spatial heterogeneity of the $P-Z$ correlation we computed a correlation coefficient between these two fields at every point of the 2D horizontal model space (Fig. 6) which is representative only of a square of 10×10 model grid points centred at each point. Similar structures occur if the calculation is carried out with 5×5 or 20×20 grid. As seen from Fig. 6a, during survey B phytoplankton and zooplankton are negatively correlated in the western part of the domain. Areas of strong positive correlation are significantly smaller and occur in the eastern part of the domain. During the next survey C (Fig. 6b) areas of strong positive and negative correlation reversed almost without change of pattern suggesting dominance of the predator–prey oscillation in the ecosystem dynamics.

Comparison of the model results with the data close to the moments of data assimilation is not informative, because model results are forced to be close to observations. 27 April has been chosen for discussion because by that time all data collected during the survey B have been assimilated and this day has the largest offset from assimilation over the duration of survey B. Model results in the eastern part of the domain are close to the data because of the last cycle of assimilation of 25 April, while for the western part of the domain all measurements lag behind in time significantly (5–8 days) for a direct comparison. The only remark that it is possible to make with confidence about phytoplankton is that the modelled field (as well as at the other days of survey B) manifests the same scale of patchiness and averaged value as the observed field; nevertheless, horizontal gradients in the modelled field are higher than were observed in Chl-*a* concentration along the cruse track within one day (cf. Fig. 3b and 5b). The opposite tendency is noted for zooplankton biomass. Measured microzooplankton manifests significant

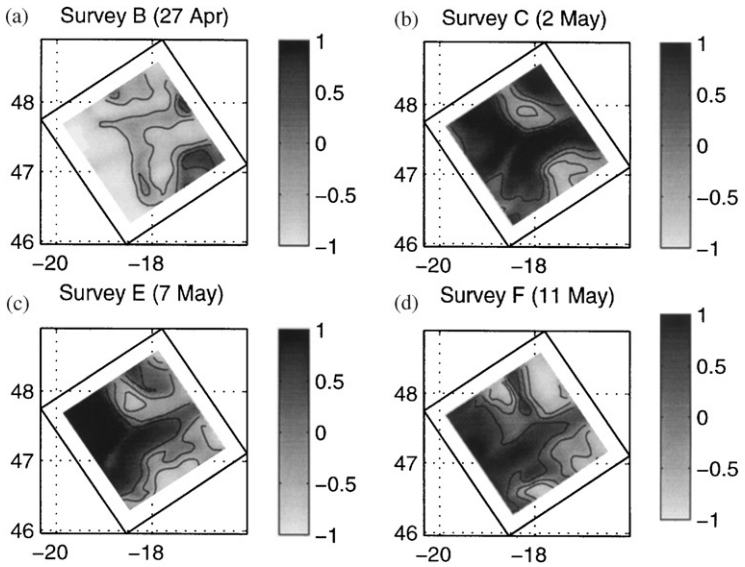

Fig. 6. Correlation (see text) between P and Z horizontal fields (depth 5 m) for 27 April (a), 2 May (b), 7 May (c), 11 May (d).

variability on spatial scales smaller than any other observed variable (Fig. 4a). Nevertheless, these zooplankton spatial gradients were smoothed in initial and assimilated fields by the objective analysis. Although some modelling studies (e.g. Steele and Henderson, 1992) show that as a result of predator–prey oscillations zooplankton patchiness can be generated on scales smaller than T and P, such patchiness has not developed in our simulation, probably because of the relatively short time scales.

Modelled depth integrated (100 m) daily primary production is shown in Fig. 5c. Its values vary by a factor of three across the model area (2.5–7.5 mmol N m^{-2} day^{-1} or about 210–630 mg C m^{-2} day^{-1}) with spatial patterns following phytoplankton distribution. The averaged value over the model area is 4.9 mmol N m^{-2} day^{-1} or 412 mg C m^{-2} day^{-1}. The f-ratio (ratio of the depth integrated (0–100 m) new production to the depth integrated (0–100 m) total primary production (Fig. 7a) varies between 0.4 and 0.85 (with the average value of 0.67), and its spatial distribution is positively correlated with phytoplankton (Fig. 5b). This fact is not surprising, because when an ecosystem is not nitrate limited, f-ratio is inversely proportional to ammonium concentration (which is usually below half-saturation level) and ammonium is in its turn directly proportional to zooplankton biomass. So when phytoplankton and zooplankton are in negative correlation with each other, spatial patterns of f-ratio follow patterns of phytoplankton. e-ratio (ratio of the export of organic material at 100 m to integrated (0–100 m) primary production) varies more significantly (0.11–1.1, with the average value of 0.42 (Fig. 7b)), following the spatial patterns of zooplankton. Modelled export of the particular organic matter at 100 m depth consists of slow gravitational sinking of detritus and fast gravitational sinking of a fraction of zooplankton losses. The latter significantly exceeds the former, so e-ratio shows clear positive correlation with zooplankton patterns. This leads to an unexpected conclusion that, although e-ratio and f-ratio are supposed to be equal to each other over long time periods, on the daily timescale they may appear to be in negative correlation.

A recent review of primary production data and estimates of f- and e-ratios for 47°N 20°W can be found in Bury et al. (2001). For the period of April–June primary production values fall in the broad range from 400 (reported for oligotrophic post-bloom conditions) to 1900 mg C m^{-2} day^{-1}. Most values reported for the spring bloom periods (years 1989 and 1990) were around 1000–1200 mg C m^{-2} day^{-1}. Our modelled production is in the range of these values but is closer to the lower limit. It is difficult to make a direct comparison of our results with observations made in 1989 and 1990 because of the very different development of the spring bloom and post-bloom situations. In both these years the peak of the phytoplankton spring bloom (with maximum of Chl-a values in excess of 3 mg Chl m^{-3} (Bury et al., 2001; Lochte et al., 1993; Ducklow and Harris, 1993) was followed by oligotrophic conditions. D227 was late for a bloom, but oligotrophic conditions were not observed and we should expect values lower than 1000–1200 mg C m^{-2} day^{-1} reported for the

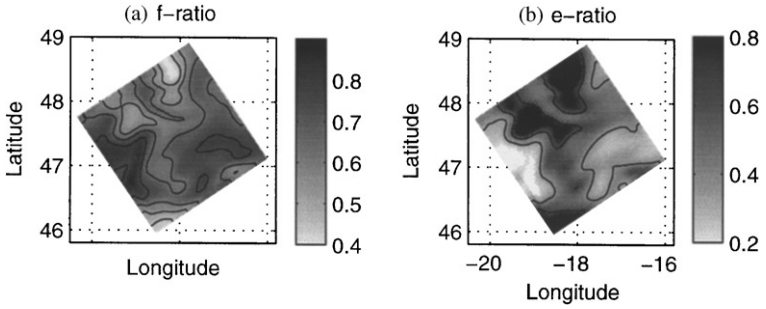

Fig. 7. Modelled horizontal fields of (a) f-ratio, (b) e-ratio for 27 April (survey B).

productivity peak in 1989 and 1990. Our modelled *f*-ratio is consistent with estimates obtained by Bury et al. (2001) for spring of 1990 (0.6–0.8 over the period of bloom development and about 0.45 as surface nitrate values decreased). Estimates of *e*-ratio available for the spring of 1989 are significantly lower than *f*-ratio and vary between 0.1 and 0.5. Our model shows the same relationship between *f*- and *e*-ratios, which should probably be typical for spring conditions.

4.2. Survey C. Shallow mixing

Between the completion of survey B (28.04.97) and beginning of survey C (1.05.97) stabilisation of the water column occurred because of the low wind speed (2–6 ms^{-1}). UML depth decreased from 50–70 m at 27–28 April to 20–40 m observed at 1–2 May (Fig. 2d). Over the same period surface temperature increased by about 1° and reached its maximum (14–14.2°C) for the cruise period. (No measurements were available for 29–30 April, when the ship was out of the survey area because of a medical emergency.) These features are well reproduced by the model (modelled results for 2 May are shown in Fig. 8).

Stabilisation of the water column stratification has disrupted the balance of nitrogen fluxes through the ecosystem which persisted during the survey B and maintained nearly constant concentrations of phyto- and zooplankton. Because of the break in surveying, we cannot say from

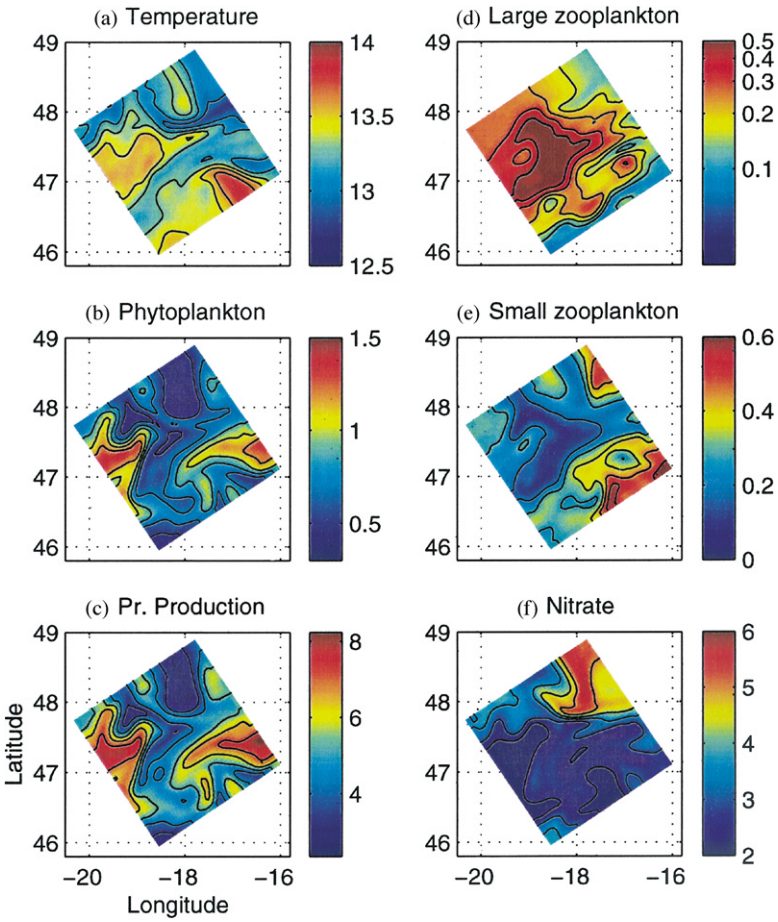

Fig. 8. The same as Fig. 5 except for 2 May (survey C).

measurements when and how fast this change occurred. Nevertheless, comparison between data collected on 25–27 April at the eastern part of the survey B and on 1–2 May over the whole area of survey C gives the following picture. In the more shallow mixed layer, increased primary production led to the increase of Chl-*a* values from 1.0–1.2 mg Chl m^{-3} to about 1.2–1.8 mg Chl m^{-3} (Figs. 2a and 3b). Small zooplankton biomass as measured by microscopic analysis and OPC increased from 0.1–0.2 to 0.2–0.3 mmol N m^{-3} (Fig. 2b). Larger (size of 500–1000 μm) zooplankton biomass also increased from about 0.02–0.05 mmol N m^{-3} to about 0.1–0.3 mmol N m^{-3}. These factors were accompanied by a fall in nitrate concentration from 3–4 to 1–2.5 mmol m^{-3} (Figs. 2c and 3c).

As seen from Figs. 2 and 8 all the features described above are well reproduced by the model except for the nitrate concentration, which remains too high (2–3 mol m^{-3} in the eastern part of the domain) for the duration of the small-scale survey. Integrated primary production averaged over the model area increased from 4.9 to 5.6 mmol N m^{-2} day^{-1} with maximum values about 8.6 mmol N m^{-2} day^{-1} (or 722 mmol C m^{-2} day^{-1}) in the southwestern and eastern parts of the domain (Fig. 8c). Averaged values of *e*- and *f*-ratios hardly changed compared with survey B, and their spatial distributions have the same features: *f*-ratio generally follows the pattern of phytoplankton, *e*-ratio follows the pattern of zooplankton.

As a result of stable stratification, primary production exceeded grazing and gave rise to a phytoplankton "mini-bloom". With nitrate concentration still above limiting values (Fig. 2c), predator–prey oscillations generated a more "patchy" structure with higher spatial gradients than during survey B (cf. Figs. 5 and 8) with the same lack of apparent correlation with temperature patterns.

4.3. Survey E. Impact of the storm

On 4 May, another small-scale survey had been started. However, because of worsening weather conditions on 5 May, this survey was abandoned. The survey was started again on 7 May.

As a result of the storm, the UML deepened from 30–40 m at the end of survey C to 70–80 m (Fig. 2d). Entrainment of nitrate increased its concentration up to 2.6–4.5 mmol N m^{-3} (Fig. 2c). Chl-*a* concentration decreased from 1.2–1.4 to 0.8–1 mg Chl m^{-3} (Fig. 2a). The biomass of both zooplankton classes did not change significantly after the storm (Fig. 2b), possibly because of the ability of zooplankton to migrate vertically.

Model results for the 7 May are shown in Fig. 9. Phytoplankton and small zooplankton concentrations decreased by about 30% because of dilution (cf. Figs. 8b and 9b, Figs. 8e and 9e). Because of the entrainment effect, the nitrate concentration increased by 1–1.5 mmol m^{-3} (cf. Fig. 8f and 9f). Because the lower integrated PAR in the deeper UML, averaged primary production decreased from 5.6 to 4.6 mmol N m^{-2} day^{-1} (or to 386 mg C m^{-2} day^{-1}, Fig. 9c) with averaged *f*- and *e*-ratios almost constant in time (changes do not exceed 2%). Nevertheless similar to surveys B and C both ratios have high spatial gradients. *e*-ratio varies from 0.11 to 1.34 with values in excess of 1 corresponding to the areas of high zooplankton concentration. In such areas (about 2% of model domain) export of organic matter from the upper layer (which consists mainly of zooplankton losses) exceeds primary production. It is interesting to note that an *e*-ratio greater than 1 is restricted to the deep UML with low values of primary production and did not occur during survey C when the stratification was very stable. The *f*-ratio varies from 0.3 to 0.8 with spatial patterns in negative correlation with *e*-ratio.

4.4. Survey F. Post-storm conditions

Large-scale survey F was carried out on 10–13 May. During this survey, UML depth was still very deep (70–80 m) with the beginning of some shallowing on the last day of the cruise (Fig. 2d). Chl-*a* concentration remained low, 0.8–1.1 mg Chl m^{-3} with larger values in the western part of the domain (Figs. 2a and 3e). Mesozooplankton (size 250–500 μm) biomass was about 0.15–0.2 mmol N m^{-3} (Figs. 2b and 4e) with spatial distribution clearly in negative correlation with

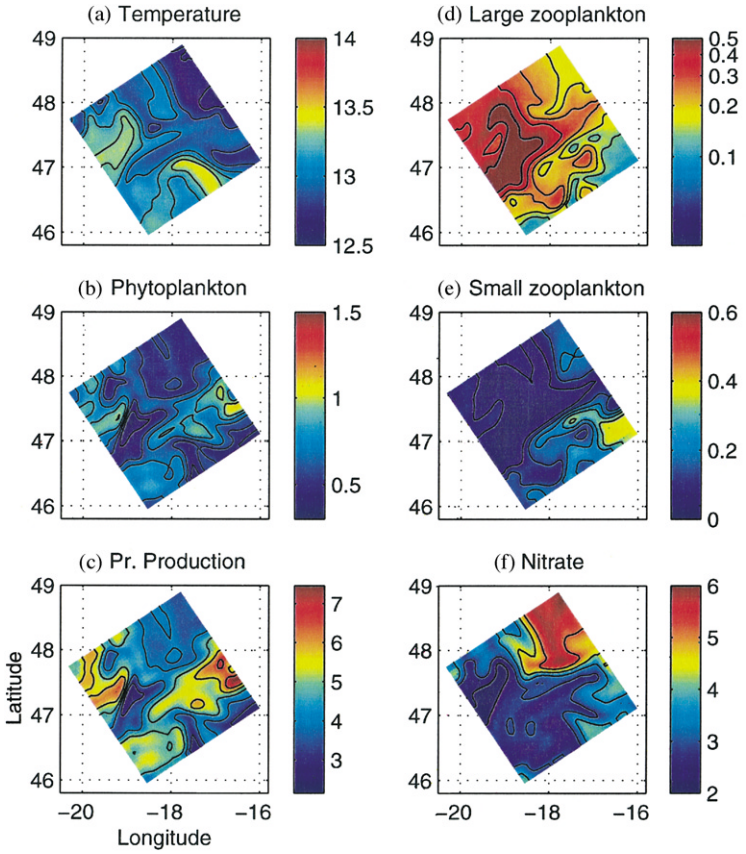

Fig. 9. The same as Fig. 5 except for 7 May (survey E).

Chl-*a*. The biomass of larger zooplankton varied between 0.1 and 0.7 mmol N m^{-3} with maximum values in the eastern part of the domain (Fig. 4f). Nitrate values were 2–4.5 mmol m^{-3} (Fig. 3d), with spatial patterns in negative coorelation with Chl-*a*. The zig-zag structure of the last two legs of the survey allowed some estimation of the change rate of the nitrate, zooplankton and Chl-*a* in the same fashion as for survey B. These estimates show that conditions were in fact very similar to those during survey B. Chl-*a* and small zooplankton were nearly constant and nitrate was declining at a rate of about 0.1–0.2 mmol m^{-3} day^{-1}. Because of the very patchy structure of the larger zooplankton in the vicinity of the leg crossings, it is difficult to estimate its rate of change.

Modelled fields for 11 May are shown in Fig. 10. Background phytoplankton values of 0.8–1.2 mmol N m^{-3} are in a reasonable agreement with data (cf. Figs. 3e and 10b). Location of the patches of high phytoplankton in the western and southern parts of the domain are reproduced correctly, but spatial gradients are overestimated. In addition to these two patches of high phytoplankton supported by data, another patch of high phytoplankton occurs in the eastern part of the domain, where measurements made at 9–10 and 13 May showed relatively low values (Fig. 3e). This modelled patch is not necessarily an artefact. Measurements in this location on the last leg (13 May) were made at noon, when Chl-*a* values may be somewhat underestimated because of the surface quenching effect.

Similar to survey C, nitrate uptake is underestimated and modelled nitrate concentration is about 0.3 mmol m^{-3} higher than observed values.

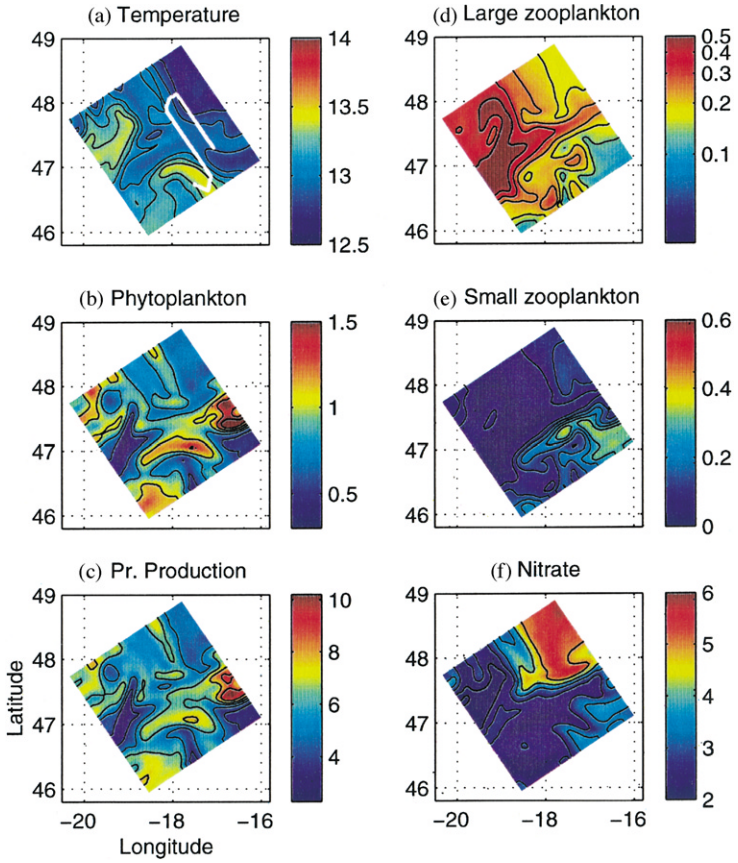

Fig. 10. The same as Fig. 5 except for 11 May (survey F). Ship position during this day is shown on the Temperature field (white line).

Despite this, spatial patterns (such as enhanced values in the northern part of the domain and low values in southern and eastern parts) are well reproduced (Fig. 10f). Agreement between and modelled zooplankton field, in the vicinity of the ship position for 11 May, with data collected during this day is reasonably good (cf. Fig. 10e and Fig. 4d and e), although modelled gradients are higher than gradients observed along the cruise track.

Depth integrated primary production averaged over the model area increased compared with the previous surveys and reached the value of 6.7 mmol $N\,m^{-2}\,day^{-1}$ (or 563 mg $C\,m^{-2}\,day^{-1}$), with maximum values of 10.8 mmol $N\,m^{-2}\,day^{-1}$ (or 907 mg $C\,m^{-2}\,day^{-1}$) in the eastern part of the domain (Fig. 10c). *f*- and *e*-ratios remained in negative correlation with each other with an averaged *f*-ratio of 0.68 and an *e*-ratio of 0.25. It is interesting to note that both ratios averaged over the model area remained almost constant during most of the cruise (varying within just 5%). The only exception is for the *e*-ratio, which decreased from 0.4 to 0.25 during the last few days. This is due to the fact that averaged small zooplankton concentration (being almost constant over the cruise) decreased during the last survey due to the increase of larger zooplankton biomass and grazing pressure on small zooplankton. Nevertheless the value of *e*-ratio during this period may be underestimated, because the model does not take into account losses of larger zooplankton, which should contribute to the export of the organic matter.

4.5. Survey F. Importance of large zooplankton

To demonstrate the importance of large zooplankton for the conditions of D227 we performed the model run without any large zooplankton grazing pressure ($q = 0$, see B). As was expected, model results for the first 17–18 days (survey B and C) were almost unaffected by this change because of the very low biomass of larger zooplankton (Fig. 4b). Modelled fields of phytoplankton, zooplankton and primary production for survey E (7 May) and survey F (11 May) are shown in Fig. 11.

Significant change of spatial patterns of phytoplankton for both surveys (E and F) are obvious as compared to the control run (cf. Figs. 9b and 11a, and Figs. 10b and 11d). Calculated correlations showed that phytoplankton fields in the control run and this numerical experiment are in negative correlation in the western part of the area (mainly in the locations of high large zooplankton biomass) and are correlated positively in the rest of the area. This complicated response is due to two main factors having an opposite effect on phytoplankton. The first is a significant (up to factor of four) increase in small zooplankton (cf Figs. 9e and 11b, and Figs. 10e and 11e) as a result of the lack of grazing pressure from larger zooplankton. This leads to a decrease in phytoplankton because of the higher grazing by small zooplankton. The second factor is a lack of large

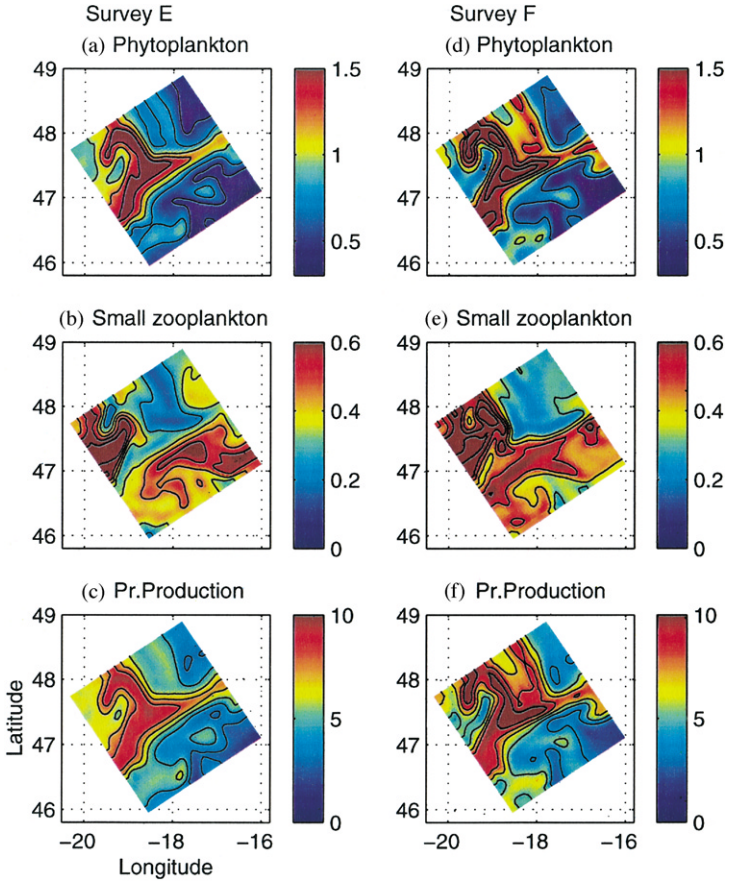

Fig. 11. Modelled horizontal fields (depth 5 m) for the run without large zooplankton grazing pressure: phytoplankton (a) and zooplankton (b) in mmol $N\,m^{-3}$ and primary production (c) in mmol $N\,m^{-2}\,day^{-1}$ for 7 May (Survey E); Phytoplankton (c), zooplankton (d) and primary production (e) for 11 May (Survey F).

zooplankton grazing on phytoplankton, which leads to an increase in phytoplankton biomass. The difference between phytoplankton in the control run and numerical experiment showed that the effect of the second factor exceeds the effect of the first one when biomass of larger zooplankton is more than 0.3–0.4 mmol $N\,m^{-3}$.

The most significant changes occur in the western part of the domain, where the biomass of large zooplankton reaches its maximum (Fig. 4f). In this area phytoplankton biomass increased from 0.5–1.2 to 0.7–2.3 mmol $N\,m^{-3}$ by the time of the last survey, and primary production increased from 5–7 to 6–11 mmol $N\,m^{-2}\,day^{-1}$. Following the dynamics of phytoplankton spatial distribution, this increase in primary production in the western part of the domain is accompanied by a decrease in the rest of the area, and the value integrated over the model domain did not change. Nevertheless, export production increased by a factor of 2.5 (averaged *e*-ratio reached the value of 0.65) because of significant increase in zooplankton biomass.

4.6. Summary and discussion

The model was run for the duration of the cruise (19 April–13 May). Data from the first survey were assimilated via optimal interpolation on 20, 22, and 25 April. The model reproduces well the dynamics of the UML as follows: moderate mixing during the first ten days (induced by the pre-cruise storm); stabilisation of the water column with UML depth 30–40 m for the period of 1–3 May; storm induced deep mixing with UML depth 70–80 m at 4–7 May; deep mixed UML (about 60–70 m) until the end of the cruise with the beginning of some shallowing on the last day (13 May).

In the choice of model structure and parameters for our control run we tried to find a minimum set of model state variables that allows us to describe general features of the ecosystem observed on D227. We have shown that a five compartment ($P-Z-N-D-A$) model can meet these requirements if mesozooplankton (500–1000 μm) is taken into account as an external tracer in addition to model variable Z describing zooplankton less than 500 μm in size.

Satellite information and microplankton species composition suggested that the spring phytoplankton peak was already over and probably occurred about 2–3 weeks prior to the cruise. Therefore, we refer to the conditions observed during D227 and reproduced by the model as "grazing controlled late-bloom period". Under these conditions, Chl-*a* concentration was relatively low (1–1.5 mg $Chl\,m^{-3}$), and phytoplankton growth was not limited by nitrate availability (whose concentration never dropped below 1 mmol m^{-3}) but was controlled by micro- and mesozooplankton grazing.

The model reproduces these features well. The modelled field of phytoplankton produces somewhat higher spatial gradients than the observed Chl-*a* distribution, although the positions of high phytoplankton patches are reproduced reasonably accurately. There are a number of possible explanations for the high modelled spatial gradients. The first is an uncertainty in Chl-*a* measurement calibration, in particular, the correction for the quenching effect, which may underestimate spatial variability. The second is that we used a constant Chl-*a* to phytoplankton ratio, but it may vary significantly over the model area (e.g. Cloern et al., 1995). The third is that the model we use may be more non-linear than the processes in the real ecosystem. It should be kept in mind that the Fasham-type model that we use was initially developed and calibrated for an annual cycle, and the application of such a model on shorter time scales may call for linearisation of some parameterisations. The fourth possible explanation is that initial conditions for zooplankton show very high spatial gradients, which disappear after a few days of the model run. These high initial gradients, which might be responsible for overestimated phytoplankton spatial variability, come from microzooplankton measurements, which are subject to some uncertainty. The first two explanations imply that the observed spatial variability of phytoplankton is underestimated, and the second two explanations point to possible overestimated modelled gradients. All four of them remain purely speculative suggestions, since our data set is not sufficient to provide an answer to this question.

Another interesting feature of the modelled patchiness is that zooplankton observations demonstrate the existence of smaller-scale structures than seen in the modelled field. One explanation is that such structures in the model are top-down controlled (i.e. controlled by the interaction between small and the larger size zooplankton). Large (500–1000 μm) zooplankton dynamics are not modelled explicitly; hence some patchiness formation mechanisms, such as zooplankton vertical migration, are not included in the model. There are suggestions of such migration in the OPC data (Srokosz, personal comm.). On the other hand, as shown by Steele (1992), patchiness of zooplankton with spatial scales smaller than that of temperature and Chl-*a* can be generated as a result of simple predator–prey oscillations and does not require complex assumptions about zooplankton behaviour. In their 1D horizontal model white noise was introduced into the zooplankton mortality term and resulted in different slopes of the power spectra for phytoplankton and zooplankton.

Modelled *f*- and *e*-ratios (integrated over 0–100 m) averaged over the area remained relatively constant over the time of the model run (varying within just 5%) with values of about 0.7 and 0.4, respectively. Nevertheless, both ratios showed great spatial variability with *f*-ratio following patterns of phytoplankton and *e*-ratio following patterns of zooplankton. Although these ratios are supposed to be equal to each other when integrated over a long time period, our model results demonstrate that during the late-bloom period, on a daily timescale, they might be in negative correlation.

The ecosystem characteristics in the simulation do not demonstrate a correlation with physical (T, S, UML depth) fields except the latitudinal trend in T and N (increase in T and decrease in N towards south). This is well supported by D227 observations. We speculate that such a correlation could be observed in the case of existence of two water masses with different biological and physical characteristics, or under conditions of nutrient limitation, when physical mechanisms of nutrient supply lead to the strong response of an ecosystem. In our case none of the above dominates, and the plankton patchiness has mainly biological origin (non-linear interactions between model state variables, e.g. predator–prey oscillations). The heterogeneity of our resulting modelled fields was partly introduced into the system through the initial conditions and partly developed by the non-linear interactions. This raises the question: what was the origin of ecosystem heterogeneity in the model initial fields (as observed at the beginning of the cruise)? According to the conception of the critical length scale (Kierstead and Slobodkin, 1953), plankton distribution in winter (under a condition of a very low phytoplankton growth rate in the deep UML) should be relatively uniform. As we know, the phytoplankton bloom occurred about three weeks prior to the cruise. Are the variability of the temperature and UML depth over the model area and non-linear ecosystem interactions acting over a 3 week time period sufficient to develop spatial heterogeneity similar to that we observed at the beginning of the cruise, starting from winter homogeneous distributions? We will try to answer this question in the next section.

The main discrepancy between modelling results and data is the underestimated nitrate uptake, especially during the period of a shallow UML. Experiments on sensitivity to the parameters associated with primary production showed that an attempt to increase primary production (hence nitrate uptake) leads either to overestimated phytoplankton or, if small zooplankton grazing is changed accordingly, to overestimated values of zooplankton. These results imply that our simple model has a missing sink of nitrogen. Lack of the description of the bacterial loop (namely bacterial consumption of ammonium) may be one explanation.

The role of sequential data assimilation applied in the model run needs to be discussed here. The initial purpose was to assimilate data collected during the first large-scale survey to eliminate the non-synopticity problem. Nevertheless, the data assimilation methodology applied had an additional advantage for some of the particular circumstances of D227, which were the following. Biomass of the large zooplankton (size 500–100 μm), being almost zero during the first large-scale survey, started to grow nearly exponentially

after the break in the measurements for the medical emergency ten days after the beginning of the cruise, thus defining two clearly different biological regimes of the ecosystem. It would be a difficult or even impossible task to find a set of parameters to describe both regimes in the framework of a simple model without making it more complex. Nevertheless, assimilation of the first large-scale survey data made in three cycles brought the model results close to observations during the first 8 days of the model run by means of optimal interpolation. This made it unnecessary to fit parameters to describe the whole cruise and allowed us to concentrate on the improvement of the model fit to data for the second part of the cruise only.

One of the very unusual features observed on D227 and in our modelling results is low Chl-*a* concentration in spite of the high nutrients (so-called HNLC conditions). Previous cruises in this location in spring reported depleted nutrients in the UML after the spring phytoplankton bloom (Bury et al., 2001; Ducklow and Harris, 1993). It is not clear whether the appearance of HNLC type conditions was a result of severe weather conditions and deep mixing (one storm occurred 2 days prior to the cruise and another severe storm with mixing down to 70–80 m occurred 2 weeks after the cruise started, in contrast to the spring of 1989 and 1990, when a stable shallow UML was observed), or whether such conditions were a result of very deep winter convection and unusually high spring concentration of nutrients (Lampitt et al., 2001). To answer this question we performed a set of numerical experiments, which will be described in the next section.

5. Sensitivity analysis

5.1. "Spring bloom" experiment

The control run shows that biological mechanisms (non-linear interactions between ecosystem characteristics, mainly predator–prey oscillation) dominate the development of plankton patchiness during the cruise period. Is this mechanism also possibly responsible for the scale and intensity of patchiness observed on D227 after the spring bloom? This patchiness should have been developed from nearly homogeneous conditions existing in the pre-spring bloom situation two-three weeks prior to the cruise. To address this question we performed experiments that simulate initial conditions in the biology prior to the spring bloom. We explore the possible evolution of a spring bloom under several physical forcing scenarios, including physical conditions typical of a spring bloom event (formation of a shallow seasonal thermocline); or with no changes in the observed physical state. Since all experiments produce similar results, we describe only the experiment with no modifications to the physical state (Fig. 12). The biological initial conditions were as follows: the phytoplankton and zooplankton horizontally homogeneous with surface values equal to 0.3 and 0.03 mmol $N\,m^{-3}$ respectively. These values were taken from the study of Fasham and Evans (1995). The vertical profiles had the same shape as the mean profiles in the initialisation for the control run; nitrate values from 200 m depth were extended up to the surface providing homogeneous distribution within upper 200 m to simulate near surface nitrate content prior to the bloom; concentration of the large zooplankton was set to zero since their existence is typical of the late stage of the bloom; the rest of the biological initial fields were reconstructed as in the control run.

The evolution of the phytoplankton and zooplankton biomass averaged over the model area during the three week simulation (Fig. 12a and b) shows a maximum of about 2.5 mmol $N\,m^{-3}$ in the phytoplankton in about 2 weeks after the beginning of the model run, and about 1.5 mmol $N\,m^{-3}$ in the zooplankton a few days later. Such a development of the spring bloom is in good agreement with observations made in spring of 1989 and 1990 (Bury et al., 2001; Ducklow and Harris, 1993). Nevertheless, in spite of the fast decline, nitrate does not get depleted (Fig. 12c) reaching the minimum of 4.5 mmol m^{-3} after two weeks and then increasing again because of the entrainment.

To eliminate the expected phase error between phytoplankton and zooplankton due in part to

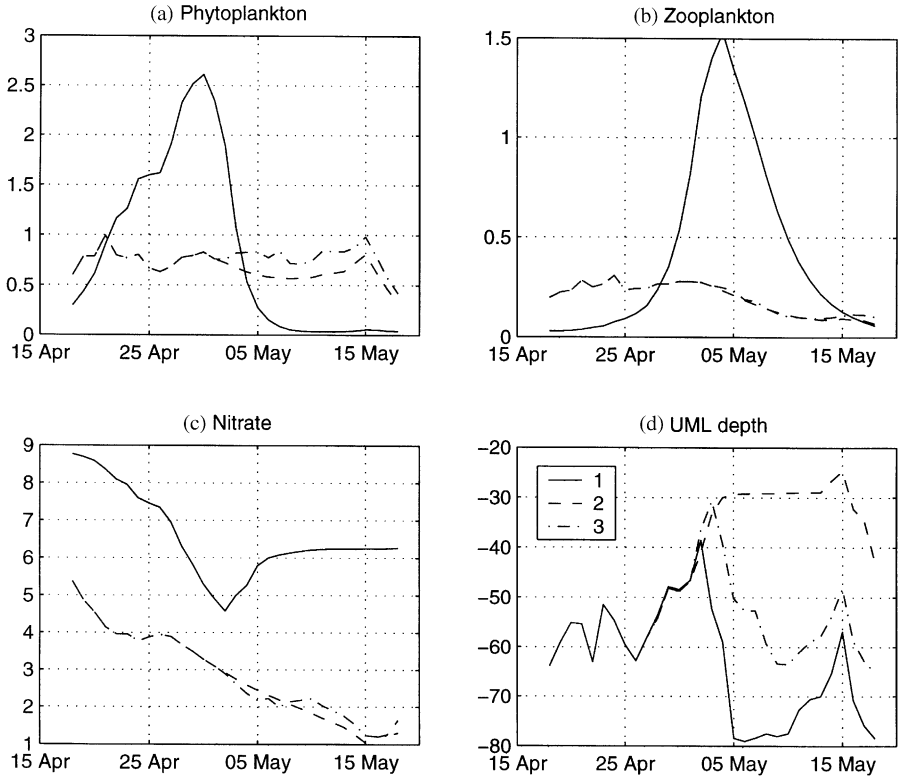

Fig. 12. Modelled evolution of the phytoplankton (a), small zooplankton (b), nitrate(c), UML depth (d), for the 5 m depth averaged over the model area for the spring bloom and sensitivity to the UML experiments: Solid line (1)—spring bloom experiment; dashed line (2)—experiment 1 (shallow mixing), dash–dotted line (3)—experiment 2 (moderate mixing).

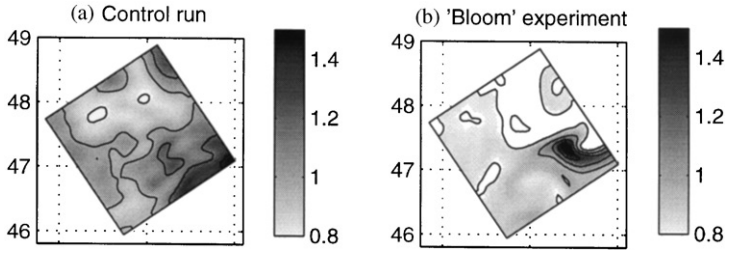

Fig. 13. Sum of the modelled zooplankton and phytoplankton fields for the depth 5 m (mmol N m^{-3}). (a) control run, (b) spring bloom experiment.

dependence in the (here unknown) evolution of the UML (Ryabchenko et al., 1998), we chose to look at the total nitrogen content of these two state variables. The sum of phytoplankton and zooplankton fields for 2 May is shown in Fig. 13b. This date corresponds to the decline of a bloom (Fig. 12a), the situation that we believe D227 found upon arrival in the area. The patchiness of this field has similar structures in size and intensity as in the beginning of the control run (sum of phyto- and zooplankton for day 5 is shown in Fig. 13a).

There are two factors responsible for the formation of the patchiness from the horizontally homogeneous initial biological fields. The first factor, playing the major role, is the significant (up to 80 m) spatial variability of the UML depth in the area (Fig. 2d) responsible for the different level of light limitation of the phytoplankton growth and different entrainment/detrainment rates on the base of the UML. The second, minor factor is the spatial temperature variability (up to 1.5°C across the area), which is responsible for only 10% variability in the phytoplankton growth rate.

5.2. Sensitivity to the UML variations

HNLC type conditions observed during the D227 cruise have not been reported for this site at this time of the year before. Spring time observations available for 1989 and 1990 show a spring phytoplankton bloom followed by nutrient depletion. During both years, the UML remained shallow during the bloom period, in contrast to D227 conditions, when two storm events, with UML deepening down to 70–80 m, occurred. To understand the role of the UML regime in the formation of HNLC conditions in 1997 we performed a sensitivity study to the external forcing.

In respect to the mixing depth, external forcing during D227 can roughly be divided into three periods (Fig. 2d): 19–29 April (moderate UML); 30 April–5 May (shallow UML); 6–15 May (deep UML). In our numerical experiments we adjusted external forcing to prevent formation of the deep UML and replaced it by: (i) a moderate UML regime (experiment 1); (ii) a shallow UML regime (experiment 2, Fig. 12d).

The evolution of the UML depth, phyto- and zooplankton and nitrate for the 5 m depth averaged over the model area for both numerical experiments are shown in Fig. 12 (cf. Figs. 2 and 12). While the dynamics of phyto- and zooplankton remain almost unchanged compared with the control run, nitrate uptake rate is different (with largest uptake in the shallow mixing regime). Nevertheless, none of the UML scenarios have a nitrate concentration by the end of the model run low enough to provide limitation of phytoplankton primary production. In both numerical experiments, at least another week of shallow UML is needed for phytoplankton to become nitrate limited. This brings us to the conclusion that deep mixing observed during a significant part of the D227 cruise period was not the only reason for HNLC conditions after the spring phytoplankton bloom. The second factor is very high nitrate concentration in the surface layer prior to the bloom as a result of winter convection significantly deeper in 1997 compared with 1989 and 1990. Such a difference is supported by the difference between nitrate concentration at 80–100 m depth (which should be a good proxy for the pre-bloom surface concentration) observed during both 1989 and 1990 bloom experiments and during D227. Values reported for 1989 were about 6–8 $\mathrm{mmol\,m^{-3}}$ (Marra and Ho, 1993; Garside and Garside, 1993); values observed on D227 for the same depth were 7–10 $\mathrm{mmol\,m^{-3}}$.

6. Final remarks

This study has demonstrated the utility of using modelling and data assimilation to interpret and understand a complex set of biological and physical observations at the mesoscale. There are major research challenges on the way to future operational applications of this approach include: first, using of the system described here at sea with the aim of optimising the cruise sampling strategy. Some initial steps in this direction are described in Popova et al. (2002). Second is the development of a more flexible biological model than the one used in this study. Such a model should be capable of coping with more complex conditions, e.g. the limitation of primary production by both nitrate and silicate, the succession of species in the transition from a diatom-dominated to a non-diatom bloom, and the effects of diurnal vertical migration of zooplankton. This is currently being implemented. Third, and not least, is the ability to obtain in near real time the biological data (e.g. microzooplankton biomass and plankton species information) that is usually available only after a cruise, as it requires labor-intensive work. This last challenge is the most difficult to meet.

Acknowledgements

This research was supported by MOD/NERC Joint Grant Scheme study (Development of techniques for assimilating biological and physical data into 3D eddy-resolving ocean circulation models). We are grateful to J.C. Scott (DERA), P.F. Lermusiaux and W.G. Leslie for many useful discussion and to L.A. Anderson for the first setup of the numerical experiment onboard D227. We would also like to thank all scientific personel and crew of the D227 cruise for the hard work in gathering the dataset used in this study. Harvard University gratefully acknowledges the support of the Office of Naval Research under the following grants: N00014-95-1-0371, N00014-97-1-0239 and N00014-95-1-0033.

Appendix A. Autocorrelation function

The objective analyses used a Gaussian autocorrelation function in space (X, Y) and time (T) of the form

$$C(X_j, Y_j, T_j, X_i, Y_i, T_i) = \left(1 - \frac{R_x^2}{x_0^2} - \frac{R_y^2}{y_0^2}\right) \times \exp\left(-0.5\left(\left(\frac{R_x^2}{x_d^2} - \frac{R_y^2}{y_d^2}\right) + \frac{t_P^2}{t_d^2}\right)\right), \quad (A.1)$$

where $R_x = x_p\cos(\phi) + y_p\sin(\phi)$, $R_y = y_P\cos(\phi) - x_P\sin(\phi)$, $x_P = X_j - X_i$, $y_P = Y_j - Y_i$, $t_P = T_j - T_i$; x_0, y_0 are the zonal and meridional zero crossings (set to 120 km), x_d, y_d, t_d are the zonal meridional and temporal decorrelation scales, ϕ is the domain rotation angle.

Appendix B. Biological model equations

The biological variables are phytoplankton P, small zooplankton Z, nitrate N, ammonium A, detritus D, and large zooplankton Z_L. Generically denoted by X, the governing equations are

$$\frac{D}{Dt}X + \frac{\partial}{\partial z}K_v\frac{\partial X}{\partial z} = B_X, \quad (B.1)$$

where D/Dt is the material derivative, K_v is the eddy vertical diffusivity co-efficient, and B_X are the source and sinks, given by

$$B_P = JP(Q_N + Q_A) - G_P - \mathrm{De}_P - G_{LP}, \quad (B.2)$$

$$B_Z = \beta_P G_P + \beta_D G_D - De_Z - E_Z - G_{LZ}, \quad (B.3)$$

$$B_D = (1-\beta_P)G_P - \beta_D G_D - \mathrm{De}_D + \mathrm{De}_P - w_g\frac{\partial D}{\partial z}, \quad (B.4)$$

$$B_N = -JPQ_N, \quad (B.5)$$

$$B_A = -JPQ_A + E_Z + \delta\mathrm{De}_Z + \mathrm{De}_D, \quad (B.6)$$

$$B_{LZ} = 0. \quad (B.7)$$

The flux terms (identified in the notation section) are given by

$$J = \frac{1}{z_{i+1} - z_i} \times \int_{z_i}^{z_{i+1}} F(I_0\exp\{-(k_w + k_c P)z\})\,dz, \quad (B.8)$$

$$F(I) = \frac{V_P\alpha I}{(V_P^2 + \alpha^2 I^2)^{1/2}}, \quad V_P = 0.65 \times 1.066^T, \quad (B.9)$$

$$Q_N = \frac{N\exp(-\Psi A)}{k_N + N}, \quad Q_A = \frac{A}{k_A + A}, \quad (B.10)$$

$$G_P = \frac{gp_P P^2 Z}{k_g(p_P P + p_D D) + p_P P^2 + p_D D^2}, \quad (B.11)$$

$$G_D = \frac{gp_D D^2 Z}{k_g(p_P P + p_D D) + p_P P^2 + p_D D^2}, \quad (B.12)$$

$$G_{LP} = qZ_L P, \quad G_{LZ} = qZ_L Z, \quad (B.13)$$

$$\mathrm{De}_P = \mu_P P, \quad \mathrm{De}_Z = \mu_Z Z, \quad E_Z = \mu_e Z, \quad \mathrm{De}_D = \mu_D D, \quad (B.14)$$

References

Anderson, L.A., Robinson, A.R., Lozano, C.J., 2000. Physical and biological modeling in the Gulf Stream region: 1. Data assimilation methodology. Deep-Sea Research I 47, 1787–1827.

Baar, H.J.W.de, Boyd, P.M., 2000. The role of iron in plankton ecology and carbon dioxide transfer of the global oceans.

In: Hanson, R.B., Ducklow, H.W., Field, J.G. (Eds.), The Dynamic Ocean Carbon Cycle: A Midterm Synthesis of the Joint Global Ocean Flux Study, International Geosphere Biosphere Programme Book Series, Vol. 5. Cambridge University Press, Cambridge, pp. 61–140, ISBN 0521 65603 6 (Chapter 4).

Bury, S.J., Boyd, P.W., Preston, T., Savidge, G., Owens, N.J.P., 2001. Size-fractionated primary production and nitrogen uptake during a North Atlantic phytoplankton bloom: implications for carbon export estimates. Deep Sea Research I 48, 689–720.

Carter, E.F., Robinson, A.R., 1987. Analysis models for the estimation of the oceanic fields. Journal of Atmospheric and Oceanographic Technology 4, 49–74.

Cloern, J.E., Grenz, C., Vidergar-Lucas, L., 1995. An empirical model of the phytoplankton chlorophyll: carbon ratio—the conversion factor between productivity and growth rate. Limnology and Oceanography 40, 1313–1321.

Conkright, M.E., Levitus, S., Boyer, T.P., 1994. World Ocean Atlas 1994, Vol. 1, Nutrients. US Department of Commerce, National Oceanic and Atmospheric Administration, Washington, DC.

Dombrowsky, E., DeMey, P., 1989. Continuous assimilation in an open domain of the Northeast Atlantic. Part I: methodology and application to AthenA-88. Journal of Geophysical Research 97, 9719–9731.

Ducklow, H.W., Harris, P.R., 1993. Introduction to the JGOFS North Atlantic Bloom Experiment. Deep Sea Research II 40, 1–9.

Edwards, A.M., Yool, A., 2000. The role of higher predation in plankton population models. Journal of Plankton Research 22, 1085–1112.

Fasham, M.J.R., 1993. Modelling the marine biota. In: Heimann, M. (Ed.), The Global Carbon Cycle. Springer, Berlin, pp. 457–504.

Fasham, M.J.R., Evans, G.T., 1995. The use of optimisation techniques to model marine ecosystem dynamics at the JGOFS station at 47°N 20°W. Philosophical Transactions of the Royal Society of London B 348, 206–209.

Fasham, M.J.R., Ducklow, H.W., McKelvie, S.M., 1990. A nitrogen-based model of plankton dynamics in the oceanic mixed layer. Journal of Marine Research 48, 591–639.

Gallienne, C.P., Robbins, D.B., Wood-Walker, R.S., 2001. Abundance distribution and size structure of zooplankton along a 20° west meridional transect of the northeast Atlantic Ocean in July. Deep Sea Research II 48, 925–949.

Garside, C., Garside, J.C., 1993. The "f-ratio" on 20°W during the JGOFS North Atlantic Bloom Experiment. Deep Sea Research II 40, 91–114.

Kierstead, H., Slobodkin, L.B., 1953. The size of water masses containing plankton blooms. Journal of Marine Research 12, 141–147.

Lampitt, R.S., Bett, B.J., Kiriakoulakis, K., Popova, E.E., Ragueneau, O., Vangriesheim, A., Wolff, G.A., 2001. Material supply to the abyssal seafloor in the Northeast Atlantic. Progress in Oceanography 50, 27–63.

Levitus, S., Boyer, T.P., 1994. World Ocean Atlas 1994, Vol. 4: Temperature. US Department of Commerce, National Oceanic and Atmospheric Administration, Washington, DC.

Lochte, K., Ducklow, H.W., Fasham, M.J.R., Stienen, C., 1993. Plankton succession and carbon cycling at 47°N 20°W during the JGOFS North Atlantic Bloom Experiment. Deep Sea Research II 40, 91–114.

Lozano, C.J., Haley, P.J., Arango, H.G., Sloan, N.Q., Robinson, A.R., 1994. Harvard coastal/deep water primitive equation model. Harvard Open Ocean Model Report No. 52, Harvard University, Cambridge, MA.

Lozano, C.J., Robinson, A.R., Arango, H.G., Gangopadhyay, A., Sloan, N.Q., Haley, P.J., Leslie, W.G., 1996. An interdisciplinary ocean prediction system: assimilation strategies and structured data models. Modern approaches to data assimilation in ocean modelling. In: Malonotte-Rizzoli, P. (Ed.), Elsevier Oceanography Series. Elsevier Science, Amsterdam, pp. 413–452.

Marra, J., Ho, C., 1993. Initiation of the spring bloom in the northeast Atlantic (47°N, 20°W): a numerical simulation. Deep Sea Research II 40, 55–74.

O'Mahony, J., 1998. RRS *Discovery* Cruise 227, 15 April–16 May 1997. Phyto-plankton and Microzooplankton. Southampton Institute, Maritime Research Centre, Southampton 100pp.

Orlanski, I., 1976. A simple boundary condition for unbounded hyperbolic flows. Journal of Computational Physics 41, 251–269.

Pacanowski, R.C., Philander, S.G.H., 1981. Parameterisation of vertical mixing in numerical models of tropical ocean. Journal of Physical Oceanography 11, 1443–1451.

Parsons, T.R., Takahashi, M., Hargrave, B.E., 1977. Biological Oceanographic Processes. 2nd Edition. Pergamon Press, New York, 332pp.

Popova, E.E., Srokosz, M.A., Smeed, D.A., 2002. Real-time forecasting of biological and physical dynamics at the Iceland-Faeroes Front in June 2001. Geophysical Research Letters 29, 14.1–14.4. DOI 1029/2001GL013706.

Rhines, P.B., 1979. Geostrophic turbulence. Annual Review of Fluid Mechanics 11, 401–441.

Robinson, A.R., 1992. Shipbord prediction with a regional forecast model. Oceanography 5, 42–48.

Robinson, A.R., 1996. Physical processes, field estimation and an approach to interdisciplinary ocean modelling. Earth-Science Review 40, 3–54.

Robinson, A.R., Lermusiaux, P.F.J., 2002. Data assimilation for modeling and predicting coupled physical–biological interactions in the sea. In: Robinson, A.R., McCarthy, J.R., Rothschild, B.J. (Eds.), The Sea, Biological–Physical Interactions in the Sea, Vol. 12, Wiley, NY, 457–536.

Robinson, A.R., Walstad, L.J., 1987. The Harvard open ocean model: calibration and application to dynamical processes, forecasting and data assimilation studies. Journal of Applied Numerical Mathematics 3, 89–131.

Robinson, A.R., Arango, H.G., Miller, A.J., Warn-Varnas, A., Poulain, P.-M., Leslie, W.G., 1996. Real-time operational

forecasting on shipboard of the Iceland-Faeroe frontal variability. Bulletin of the American Meteorological Society 77 (2), 243–259.

Ryabchenko, V.A., Fasham, M.J.R., Kagan, B.A., Popova, E.E., 1997. What causes short-term oscillations in ecosystem models of the ocean mixed layer? Journal of Marine Systems 13, 33–50.

Ryabchenko, V.A., Gorchakov, V.A., Fasham, M.J.R., 1998. Seasonal dynamics and biological productivity in the Arabian Sea euphotic zone as simulated by a 3-D ecosystem model. Global Biogeochemical Cycles 12, 501–530.

Shapiro, R., 1970. Smoothing, filtering and boundary effects. Review of Geophysics and Space Physics 8 (2), 359–387.

Spall, M.A., Robinson, A.R., 1989. A new open ocean, hybrid coordinate primitive equation model. Mathematics and Computers in Simulation 31, 241–269.

Srokosz, M.A., 1997. RRS *Discovery* Cruise 227, 15 Apr–16 May 1997. Plankton patchiness studies by ship and satellite: P^2S^3. Southampton Oceanography Centre Cruise Report, Southampton, 76pp.

Steele, J.H., Henderson, E.W., 1992. A simple model for plankton pathchiness. Journal of Plankton Research 14, 1397–1403.

Strass, V., 1990. On the calibration of large-scale fluorimetric chlorophyll measurements from towed undulating vehicles. Deep-Sea Research I 37, 525–540.